REVIEWS

A functional NMR for membrane proteins: dynamics, ligand binding, and allosteric modulation

Kirill Oxenoid and James J. Chou*

Department of Biological Chemistry and Molecular Pharmacology, Harvard Medical School, Boston, Massachusetts 02115

Received 8 February 2016; Accepted 25 February 2016
DOI: 10.1002/pro.2910
Published online 1 March 2016 proteinscience.org

Abstract: By nature of conducting ions, transporting substrates and transducing signals, membrane channels, transporters and receptors are expected to exhibit intrinsic conformational dynamics. It is therefore of great interest and importance to understand the various properties of conformational dynamics acquired by these proteins, for example, the relative population of states, exchange rate, conformations of multiple states, and how small molecule ligands modulate the conformational exchange. Because small molecule binding to membrane proteins can be weak and/or dynamic, structural characterization of these effects is very challenging. This review describes several NMR studies of membrane protein dynamics, ligand-induced conformational rearrangements, and the effect of ligand binding on the equilibrium of conformational exchange. The functional significance of the observed phenomena is discussed.

Keywords: ion channels; transporters; membrane receptors; protein dynamics; drug binding; allosteric modulation; NMR

Introduction

Universally appreciated as an extremely important class of biological molecules, membrane proteins (MP) have for a long time remained poorly understood from the structural perspective. By the turn of this century, only a handful of high resolution MP structures had been solved, as compared to thousands of water-soluble proteins. However, starting with a spectacular structure of the potassium channel,[1] scientists began making serious inroads into the unexplored territory of membrane protein structural space. The following years have been marked by an exponential growth of the number of MP structures. X-ray crystallography has proven to be the most productive technique, followed by electron microscopy and nuclear magnetic resonance (NMR) spectroscopy.

The focus of this review will be on solution NMR that allows to study not only the structure of membrane proteins, but also their dynamic properties that scientists have come to recognize as critical for MP function. Examples of NMR-derived structures can now be found in all major functional groups of membrane proteins: enzymes, receptors, regulators, channels and transporters.[2–10] Solution NMR has benefited significantly from improvements both in spectroscopy (higher magnetic field,

*Correspondence to: J. J. Chou; Harvard Medical School, Biological Chemistry and Molecular Pharmacology, 250 Longwood Avenue, SGM 109, Boston, MA 02115.
E-mail: james_chou@hms.harvard.edu

cryoprobe technology, and new pulse sequences) and protein biochemistry (new isotope labeling schemes and the use of more effective membrane mimetics).

A very attractive feature of solution NMR is that it allows one to probe protein structures in the state of dynamic equilibrium. For example, it is widely recognized that ion channels can exist in multiple conformations (closed, open, inactive, etc.) and that their functional properties can be characterized by transitions between these conformations. Because NMR allows one to measure conformational dynamics at residue-specific details, it is a valuable tool for understanding channel function from the dynamics point of view. Understanding the dynamic nature of MPs is also critical for our ability to develop small and large molecule drugs, as their action may depend on conformational specificity. Another important aspect of MP dynamics is physical availability of active conformations for structural interrogation. Despite being functionally very important, active states of many membrane proteins, such as GPCRs, are often weakly populated and therefore challenging to capture by crystallography or electron microscopy, whereas NMR is sensitive enough to detect population levels of just a few percent.[11,12] Finally, because ligand binding can change the dynamic landscape of a protein, NMR is an excellent technique to probe subtle effects of ligands which do not necessarily lead to major conformational rearrangements, but can nevertheless affect the equilibrium and modulate protein function (e.g., allosteric modulation).

In this review, we discuss examples in which solution NMR applications provide new information on ligand binding and conformational exchange for a variety of membrane proteins with the focus on ion channels, transporters, and GPCRs. We first consider the use of NMR in the study of functionally relevant dynamics of MPs observed on different time scales. We then consider the effect of ligand binding on dynamics and the role of allostery in modulating conformational exchange. The last section of this review outlines some challenges presented to the researchers by the dynamic nature of traditional protein-detergent systems and emerging strategies for overcoming current limitations and allowing the study of MP dynamics in a more native-like environment.

NMR Studies of Conformational Dynamics

Dynamic properties of a potassium channel

In this section, we will consider several NMR studies of conformational dynamics at different time scales. As mentioned earlier, determination of tetrameric KcsA crystal structure marked the beginning of a new era in MP structural biology. In a series of NMR studies, Chill *et al*. have complemented previous crystallographic works with an investigation of KcsA dynamics.[13] Because KcsA remains tetrameric even in SDS detergent micelles, the first challenge the authors faced was to assign the backbone resonances in the 68 kDa complex. Although protein expression in deuterated media is a valuable approach that allows backbone assignment of large molecules, it created a major difficulty for the assignment of KcsA, because its transmembrane (TM) regions contained a large number of nonexchangeable amide sites. This problem was overcome by producing two protein samples, $Kcsa^{E}$ and $KcsA^{TM}$, for the observation of exchangeable and nonexchangeable protons, respectively. A combination of amide exchange in H_2O and D_2O and strategic amino acid labeling allowed the assignment of almost all nonproline residues and relaxation measurements for 70% of backbone resonances of the KcsA tetramer.

By measuring T_1, $T_{1\rho}$, steady-state ^{1}H–^{15}N NOE, and ^{15}N cross-correlated relaxation, the authors were able to conduct a thorough analysis of KcsA dynamics, including determination of the generalized order parameter S^2 and the time of fast internal dynamics.[13–15] The analysis revealed four regions of different dynamic behavior: (1) flexible termini, (2) intracellular membrane interface with increased rigidity towards the TM helices, (3) TM region with highest rigidity, consistent with its structural role as the framework for the assembly, and (4) extracellular region including the ion pore domain with intermediate rigidity. Interestingly, S^2 values for the ion selectivity filter are only slightly lower than those for the TM helices, indicating a rigid structure in the closed state of the channel. However, in the presence of calcium, the filter shows chemical exchange on the submillisecond scale,[14] suggesting an increase in dynamics which may be required for ion conduction.

Slow conformational exchange in a multidrug transporter

Conformational exchange could be a general property of many channels and transporters and can be seen, perhaps, most clearly in the case of a bacterial transporter EmrE. EmrE of *E. coli* is a small multidrug resistance transporter capable of expelling polyaromatic cations from the cytoplasm via the antiporter mechanism: one cation per two protons.[16] The cryo-EM and crystal structures of EmrE revealed an unusual topology—an antiparallel homodimer.[17,18] According to a single-site alternating access model, the transport occurs as the dimer cycles between an inward- and an outward-facing state. To test this model, Morrison *et al*. investigated by NMR the conformational dynamics of EmrE in bicelles.[19] The model presumes that the conformational change occurs while the substrate is bound,

therefore TPP^+, a polyaromatic substrate was added to the NMR sample. This produced a ^1H-^{15}N TROSY spectrum with two sets of peaks. The authors performed a TROSY-selected ZZ-exchange experiments and observed the cross-peaks connecting amide peaks from the two sets, thus demonstrating that the protein slowly alternates between two conformations. The analysis of peak volume as a function of mixing time in the ZZ-exchange revealed equal population of the two states. This is in agreement with the antiparallel nature of the homodimer which implies that the states are related by a pseudo-twofold symmetry and therefore have same energy. Mapping of NMR assignment onto the crystal structure revealed that the chemical exchange is wide spread and exchange measurements showed that interconversion occurs with a single frequency of $\sim 5\ s^{-1}$. The extent of conformational change can be inferred from overlaying the crystal structures of two subunits of the dimer. This agrees well with chemical shifts observed in the TROSY spectra for the two states, with largest shifts corresponding to the kinking of TM3 and shifting of TM4. In addition, paramagnetic broadening by gadolinium shows differential broadening for the two states precisely for residues from the loop and pore regions, as in each subunit they are expected to have conformation-dependent exposure to water. The described NMR study was the first of its kind, demonstrating the mechanism of an antiparallel homodimeric transporter in membrane and at the same time validating the alternating access model.

Dynamic equilibrium in a bacterial porin

In the case of EmrE transporter, the antiparallel nature of the assembly meant that a single crystal structure yielded the information on both states of the transporter. Such a fortuitous situation is rare. Most of the time, different conformations are not symmetry related and therefore separate crystal structures have to be obtained to understand conformational change. However, even when such structures are available, their mechanistic interpretation is not always straightforward, as crystal structures represent discrete states and do not provide information on the dynamic equilibrium. One case in point is a bacterial outer membrane protein OmpG, a pH-dependent β-barrel porin responsible for sugar uptake. It was crystallized at two different values of pH, 7.5 and 5.6, corresponding to open and closed states, respectively.[20] The major difference between the two structures was in the position of the extracellular loop 6 which, in the low pH structure occluded the pore. It therefore appeared that reorientation of this loop was responsible for opening and closing the channel. However, despite electrophysiological evidence of the dynamic equilibrium between the two states,[21] the link between functional data and potential loop dynamics was yet to be demonstrated. In their NMR study, Zhuang *et al*. used paramagnetic relaxation enhancement (PRE) to address the role of loop dynamics in OmpG function.[22]

Due to intermediate exchange broadening, some flexible regions, including the majority of loop 6, were missing NMR connectivities in the samples of OmpG in detergent micelles. Using selective amino acid labeling, it was possible, however, to partially assign loop 6 and determine by relaxation-dispersion experiments that it exhibited submillisecond time scale dynamics. It was also shown by the analysis of secondary chemical shifts that the loop was becoming more disordered at higher pH, which was consistent with the loop disengaging from the barrel. To enable structural analysis of extracellular loops despite insufficient assignment, the authors measured PRE effect from several MTSL paramagnetic labels positioned in the extracellular loops on more rigid regions of the β-barrel. Using the ensemble approach[23] to analyze PRE data, the authors showed that at pH 6.3 experimental PRE data agree well with back-calculated theoretical values assuming the presence of three conformers. At pH 6.3, extracellular loop 6 position varied the most among these conformers (loops 4 and 5 varied the least). Conformer 1 had loop 6 inside the pore, conformers 2 and 3—outside, with the loop in conformer 3 flipping farther out. PRE analysis showed that loop 6 sampled both open and closed conformation and the population distribution at different values of pH matched well electrophysiology measurements. Therefore, it could be concluded that the effect of pH was in shifting the existing dynamic equilibrium between an open and a closed state rather than in inducing a conformational change.

Ground and excited states of a transmembrane reductase

Large conformational dynamics was also observed by NMR in the electron transport protein CcdA. Bacterial CcdA is a TM reductase with two redox-active cysteines that transfers electrons across the inner membrane to maintain the proper redox state of periplasmic proteins.[24–26] Williamson and Cho *et al*. generated NMR spectra of the reduced and oxidized state in DPC micelles and found that they are completely different and the change is reversible,[9] suggesting that the protein is functionally competent in this detergent [Fig. 1(A)]. To capture the structure of the reduced state, a Cys-less CcdA mutant was generated whose spectrum was found to be very similar to the spectrum of wild type in the presence of a reducing agent. The structure of the Cys-less mutant was solved using NOE-derived distance restraints and validated by PREs. The structure consists of six TM helices surrounding a broken

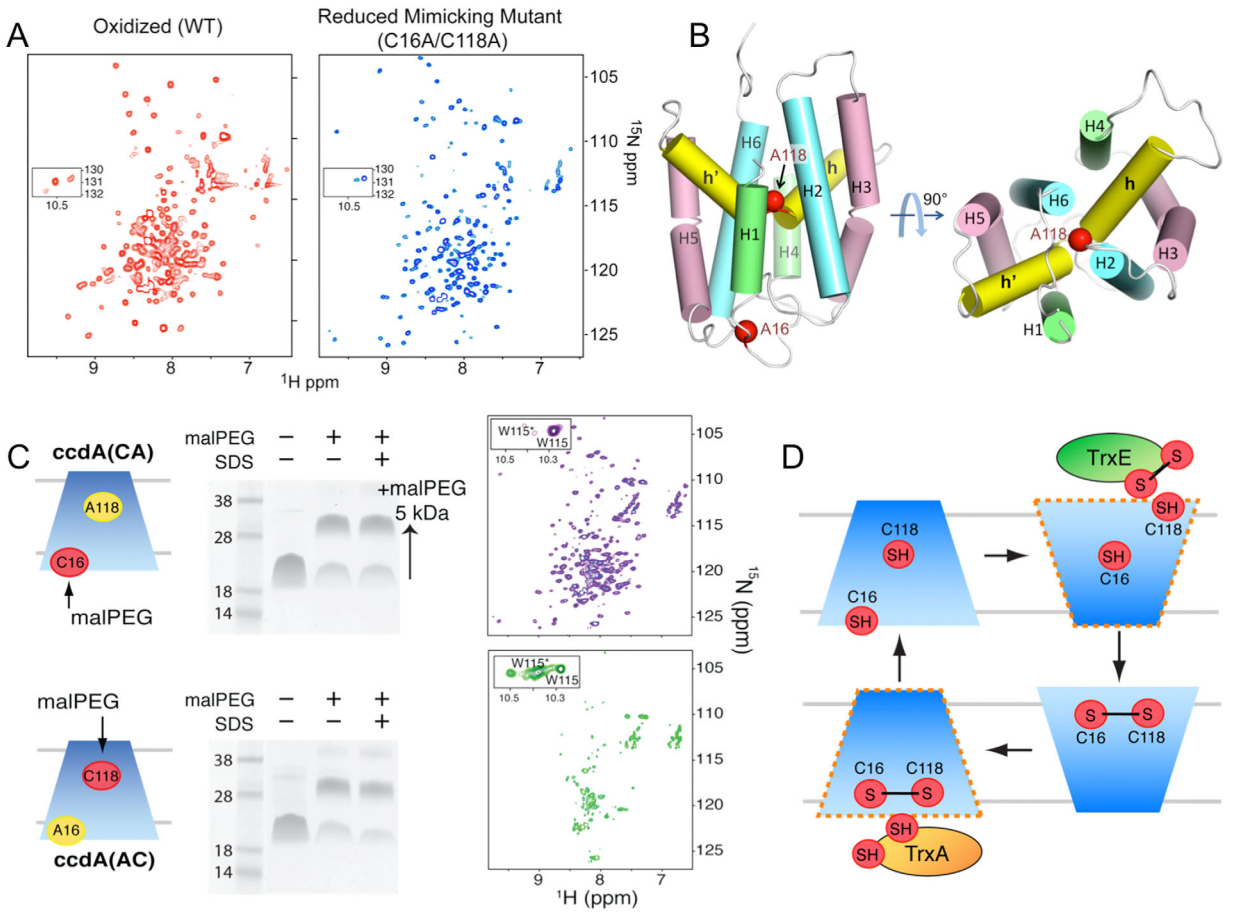

Figure 1. Conformational dynamics of the CcdA electron transporter revealed by NMR. (A) Simple comparison of the 2D ^{1}H–^{15}N TROSY–HSQC spectra of the oxidized (disulfide bonded) WT CcdA and the reduced state mimicking mutant (two Cys mutated to Ala) showed that the two forms have very different conformations. (B) The NMR structure of the putative reduced state resulting from the substitution of cysteines 16 and 118 with alanine (shown as red spheres). (C) Cysteine accessibility by malPEG labeling for the C16A and C118A mutants showed that whereas C16 is readily accessible to malPEG in the reduced state, the buried C118 is transiently accessible via an excited reduced state. (D) The proposed four-state mechanism for the transmembrane reductase.

horizontal helix on the periplasmic side, with the C118A mutation at the break dipping into the hydrophobic core of the protein [Fig. 1(B)]. The other mutation, C16A, appears in a loop region on the cytoplasmic side. Thus, in a reduced state, the two cysteines are as much as 20 Å apart. This suggests that a global conformational change is required to transition from the oxidized to the reduced state, consistent with dramatic spectral differences between the two conformations.

As expected, the cytoplasm-facing C16 was more accessible for modification by a 5 kDa hydrophilic malPEG molecule than the buried C118. Interestingly, the former modification did not significantly alter the spectrum, whereas labeling of C118 caused a dramatic spectral broadening, pointing to the existence of structurally unstable excited state of the transporter, in which C116 moves towards the periplasm and interacts with the electron acceptor protein [Fig. 1(C)]. Although reduced CcdA exists in a ground state, it appears to sample the excited state, as could be inferred from the analysis of relative intensities of two TROSY peaks corresponding to the indole moiety of W115 in the vicinity of C118. Assuming that in its oxidized form CcdA has a ground and an excited state as well, its functional cycle can be described by a four-state model [Fig. 1(D)]. (i) After reduction by the electron donor TrxA, CcdA is in a ground reduced state which is open to the cytoplasm. (ii) Although in the ground reduced state, CcdA transiently samples an excited reduced state that is periplasm-open and this state is stabilized by the binding of the electron acceptor TrxE. (iii) Oxidation of CcdA causes it to further rearrange into a ground oxidized state. (iv) The oxidized state, which is periplasm-open, also transiently samples an excited oxidized state that is again cytoplasm-open. Binding to TrxA stabilizes CcdA in the excited oxidized state and primes it for the following reduction. This mechanism for electron transport is similar to the alternating-access models describing the function of many transporters, including the

aforementioned EmrE. In the case of CcdA, however, NMR data point to the existence of two excited states, in addition to two ground states.

Small Molecule Binding

MPs account for over half of the pharmaceutical drug targets[27] and are fueling the interest to methods that can provide structural information on MP-drug interaction for the development of more potent therapeutics. The versatility of solution NMR has been proven in studying protein-ligand interactions[28] and thus should be capitalized on for investigating drug binding to MPs. The simplest application is chemical shift titration. Since chemical shifts are exquisitely sensitive to small molecule binding, NMR titration can be applied to study even the weak binders, for example, with $K_D > 100$ μM. Chemical shift perturbation is, however, an indirect indication of substrate binding because it can arise from physical proximity of the drug to the residues in question or from a binding-induced change in protein conformation or dynamics. A more accurate pinpointing of the drug binding site would thus require measurement of MP-drug NOEs, which, in turn, requires stronger binding affinity, for example, nM–μM K_D.

While NMR titration is a fast way to obtain binding information, caution needs to be taken to address several complications associated with membrane-mimetic media used for MP solubilization. First, many small molecule inhibitors are hydrophobic and preferentially partition into detergent micelles or lipid/detergent bicelles. In theory, this partitioning increases the local concentration of drug molecules available for MPs to bind. But, in real application, it is often mandatory to have a large excess of empty micelles or bicelles in order to keep the MP monodispersed at NMR friendly concentrations (>0.3 mM). Consequently, a large fraction of drug is sequestered by free micelles or bicelles. The hydrophobic partition potential of small molecules can be estimated using the octanol/water partition coefficient or predicted computationally (e.g., the Open Babel program[29]), although in some cases such estimation is inadequate as small molecules could also interact with detergent and lipid head groups. More accurate partition coefficient in micelles or bicelles can be derived using, for example, NMR diffusion measurement.[30] Accurate determination of partition will allow estimation of the effective concentration of the drug available for protein binding. Second, it is beneficial to examine drug binding under the NMR sample condition using isothermal titration calorimetry (ITC) because ITC permits the use of lower protein and detergent concentrations. Micelle or bicelle partitioning of the drug also poses technical problems to ITC. For example, if the detergent concentration of the MP sample is different from that of the titrating drug solution, detergent mismatch and detergent–drug interaction during mixing could release or absorb heat independent of the protein. It is therefore important to carry out the necessary controls to subtract these artifacts. Finally, we must acknowledge that the membrane mimetic media compatible with high resolution structural studies in most cases cannot fully reconstitute the native environment in cells. Unfortunately, whether and how these media influence the structure and function of MPs cannot be predicted and is case dependent. In general, by nature of being more dynamic assemblies, detergent micelles do not provide as much lateral pressure as MPs experience in a lipid bilayer. For MPs that are structurally less stable, drug binding in detergent micelles could be weaker simply due to increased structural dynamics around the binding site. Furthermore, free detergent molecules might sometimes interfere with drug binding. This, of course, is not a general argument against the use of detergent micelles. For MPs that can only be effectively solubilized in micelles, NMR can provide reliable information on where the drug binds, but the binding affinity might be significantly lower than under native conditions. As long as the binding site can be validated by functional mutagenesis, the structural information will be valuable to, for example, targeted *in silico* screen of small molecules, to identify stronger binders. We describe below several examples in which relatively simple NMR applications have provided critical information on small molecule binding to ion channels and transporters.

Drug binding to viral ion channels

The adamantane compounds such as amantadine and rimantadine are known to inhibit multiple viroporin proteins. The amantadine (Symadine) or rimantadine (Flumadine), which inhibit proton conduction of the influenza A M2 channel, were the first licensed drugs for treating influenza infections.[31] Rimantadine has also been shown to inhibit the p7 channel encoded by the hepatitis C virus (HCV), though with lower efficacy.[32,33] The same drug blocking two different channels from different viruses seemed fortuitous while raising an intriguing mechanistic question. The small and dynamic viral channels had presented serious challenges to structural biologists for decades. Finally, in 2008, solution NMR and crystallographic studies determined the atomic resolution structure of the TM domain of M2.[10,34] In the case of the crystallographic study in the presence of amantadine, a drug density inside the channel near residue Ser31 was found, but at resolution of 3.5 Å, it was difficult to confirm the position of amantadine binding.[34] Subsequent solid-state NMR measurements of the TM domain in lipid bilayer showed that rimantadine indeed bound

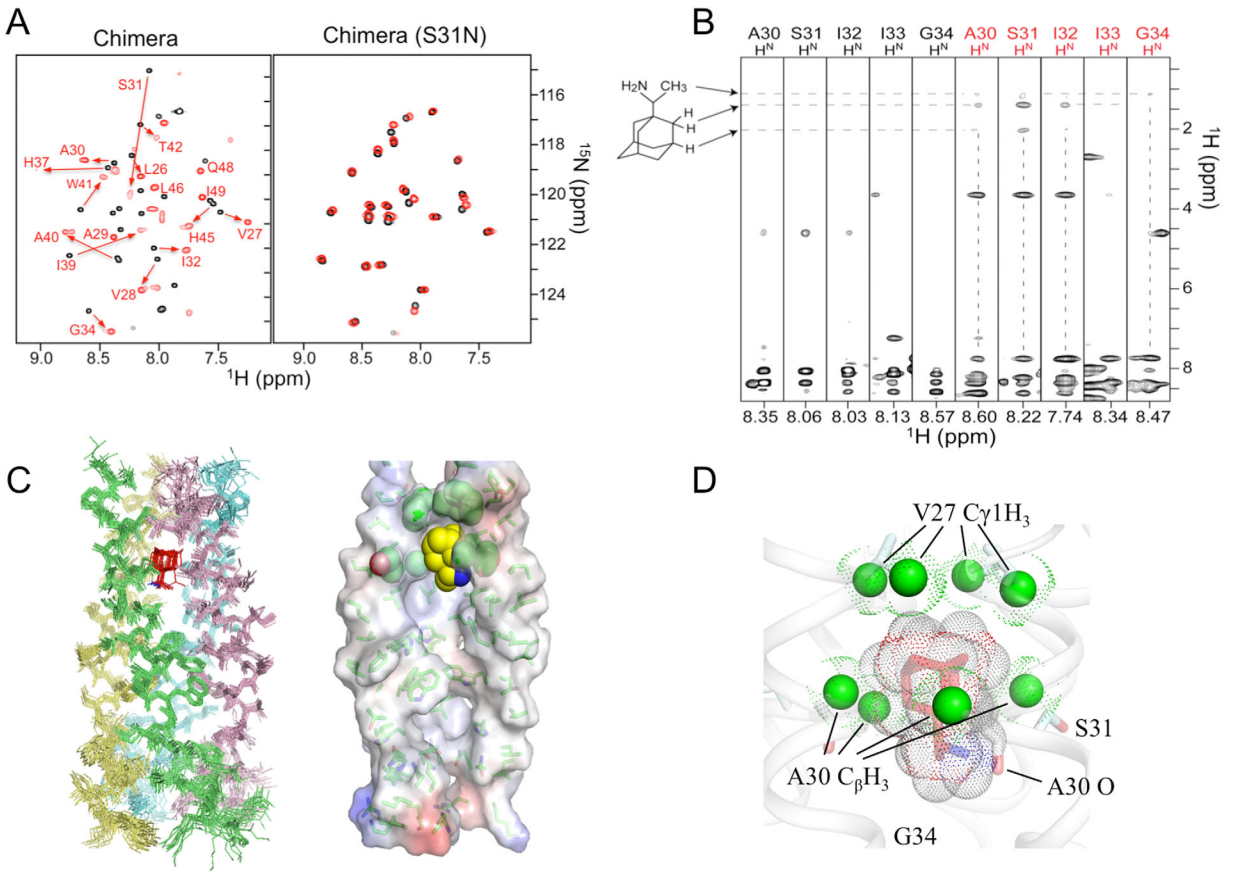

Figure 2. NMR characterization of rimantadine binding to the flu channel. (A) The 2D ^{1}H–^{15}N TROSY–HSQC spectra of the AM2-BM2 chimera channel (left panel) and the chimera channel with the drug resistant S31N mutation (right panel). Both panels show overlay of the spectra of channels reconstituted in DHPC micelles in the absence (black) and presence (red) of 50 m*M* rimantadine. Note that the high concentration of the drug was used to account for the extremely high detergent concentration (300 m*M*). (B) Selected strips from the 3D ^{15}N-edited NOESY–TROSY–HSQC spectrum recorded using the (^{15}N, ^{2}H)-labeled protein in the presence of 50 m*M* rimantadine. The strips corresponding to the drug-bound resonances are labeled in red. (C) Atomic resolution NMR structure of the chimeric channel in complex with rimantadine. The structural ensemble is shown on the left. The surface representation of the channel interior (revealed by removing one of the four subunits) shows the snug fitting of rimantadine in the internal pocket. (D) Hydrophobic and polar interactions between rimantadine and protein. The eight methyl groups (four $C^{\gamma 1}H_3$ from Val27 and four $C^{\beta}H_3$ from Ala30) that are in VDW contacts with the adamantane cage of rimantadine are shown as green balls.

to a site inside the pore[35] but still lacked sufficient structural restraints to pinpoint the precise mode of binding.

By using a chimera protein construct that contained the N-terminal half of influenza A TM (residues 18–37) and the C-terminal half of influenza B TM domain (residues 20–34),[36] Pielak *et al*. eventually obtained by solution NMR a high resolution view of rimantadine binding.[37] This construct, named (AM2–BM2)^{TM}, formed a channel that recapitulated essentially all known properties of proton conduction, drug binding, and drug resistance of the wild-type M2.[37] Upon titrating the (AM2–BM2)^{TM} in DHPC micelles with rimantadine, a new set of NMR peaks emerged and they were highly distinct from the drug-free spectrum [Fig. 2(A); left panel]. As a negative control, the chimera with the S31N mutation known to confer resistance was used, which did not show spectral changes upon the addition of rimantadine [Fig. 2(A); right panel]. For measuring exclusively NOEs between the protein and the drug, a ^{15}N-edited NOESY spectrum was recorded using a sample in which (AM2–BM2)^{TM} was ^{15}N-labeled and deuterated at the nonlabile sites and the detergent was also deuterated. In the presence of 50 m*M* rimantadine, about 60% of the chimeric channels were drug-bound and 40% unbound, as judged by the relative intensities of the NMR peaks. In this case, the NMR resonances of the drug-free population served as an internal negative control. NOE analysis immediately showed that amide protons of Ala30, Ser31, and Ile32 had intense NOE cross peaks to the adamantane CH_2 and CH protons, whereas the peaks of the unbound population did not [Fig. 2(B)]. In addition to backbone NOEs, ^{13}C-edited NOESY of uniformly ^{15}N- and ^{13}C-labeled

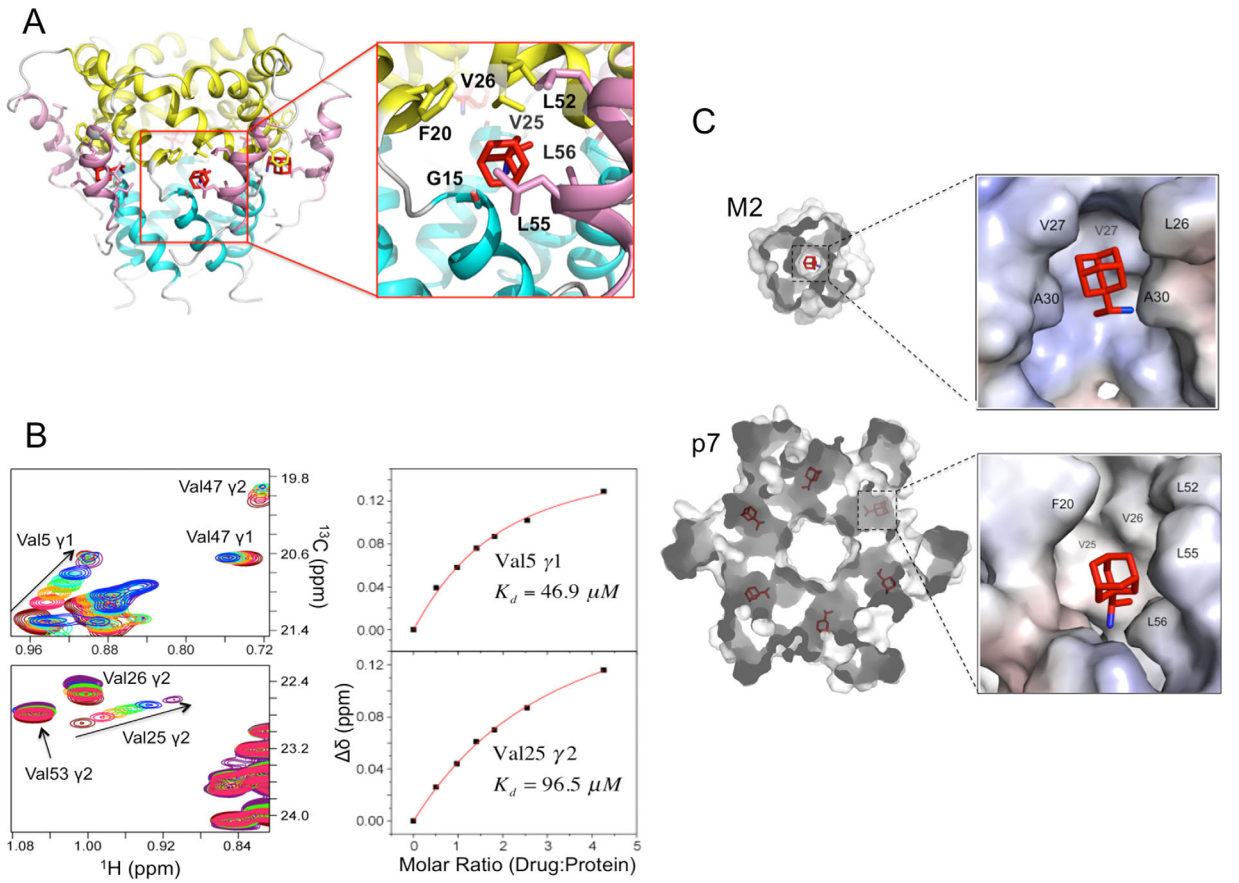

Figure 3. A different mode of rimantadine inhibition of the p7 channel. (A) p7 channel structure (left) and the rimantadine binding site (right) modeled based on the protein-drug NOEs. The H1, H2, and H3 helical segments discussed in the text are shown in cyan, yellow, and pink, respectively. (B) Rimantadine titration at very low protein and detergent concentrations. *Left*: Overlay of two regions of the ^{1}H–^{13}C HSQC spectra recorded at different rimantadine concentrations showing specific shifting of Val25 γ2 and Val5 γ1 methyl resonances. In this titration, the sample contained 38 μ*M* p7 (monomer) and 3 m*M* DPC. The p7 was (^{1}H-/^{13}C)-labeled at the methyl positions of alanines, valines and leucines but was otherwise (^{2}H-/^{12}C) labeled. The titration protocol involved addition of 0, 10, 20, 30, 40, 60, and 120 μL drug stock solution to 250 μL protein solution. *Right*: Plots of chemical shift change versus rimantadine concentration for Val25 γ2 and Val5 γ1 methyl resonances. Fitting of titration data to standard equilibrium binding equation yielded apparent K_d of 96.5 and 46.9 μ*M* for Val25 γ2 and Val5 γ1 methyl groups, respectively. (C) Comparison of the rimantadine binding sites between influenza M2 and HCV p7 channels.

protein was used for identifying NOEs between the protein methyl groups and the drug. The two sets of NOEs defined the rimantadine binding site inside the channel near residue positions 27–31: eight methyl groups of the M2 tetramer (two from each subunit: Val27 CH_3, and Ala30 CH_3) together form an internal pocket into which the adamantane cage of the drug fits snuggly [Fig. 2(C,D)]. The binding site also provided explanations for the known resistance mutations. We note that the WT AM2 (residues 18–60) reconstituted in the same DHPC micelles under the same rimantadine concentration did not bind the drug inside the channel pore.[10] Hence, a detergent should not be assumed *a priori* as being denaturing or nondenaturing because its suitability as a membrane mimetic medium strongly depends on the protein or protein construct.

In addition to blocking the influenza channel, rimantadine has also been shown to exert an inhibitory effect on the HCV p7 channel.[32,33] The viroporin p7 has been pursued as a potential therapeutic target for drugs against HCV infection.[33,38] It is a 63-residue protein that oligomerizes in membrane to form ion channels with cation selectivity.[32,39] p7 forms a 42 kDa hexamer that has a funnel-like architecture with six minimalist chains, each containing three helical segments, H1, H2, and H3 [Fig. 3(A)].[6] The H1 and H2 helices of each monomer form the narrow and wide parts of the funnel, respectively, and the H3 helix wraps around the funnel from the outside. Ouyang *et al*. performed drug titration using the p7 from genotype 5a (p7 (5a)) reconstituted in DPC micelles.[6] To minimize the detergent effect on drug binding, the sample contained only 38 μ*M* p7(5a) (monomer) and 3 m*M* DPC. Despite a low (by NMR standards) protein concentration, reasonably intense ^{1}H–^{13}C HSQC spectra of the methyl groups could be recorded at various

rimantadine concentrations. A simple titration showed a very large movement of Val25 [Fig. 3(B)], indicating fast exchange in drug binding, and data fitting yielded K_D ~96 μM. ITC of a similar sample showed K_D ~64 μM.[6] NMR titration of a micromolar sample was made possible by using the cryogenic NMR probe and the ALV-labeled protein (^{1}H-, ^{13}C-labeled at the methyl positions of Ala, Val, and Leu but otherwise deuterated, which removed the one-bond ^{13}C–^{13}C J coupling to permit the use of the more sensitive regular ^{13}C evolution). NOE experiments similar to those described for M2 were performed here to define p7–drug interaction and they revealed that rimantadine was bound to six equivalent hydrophobic pockets (due to the sixfold symmetry of the channel) between the pore-forming and peripheral helices [Fig. 3(A)]. In each site, Leu52 and Leu56 from H3 of the i monomer, Val25 and Val26 from H2 of the i + 2 monomer, and Phe20 from H2 of the i + 3 monomer form a hydrophobic pocket that holds the adamantane cage of the drug.

Comparison of the rimantadine binding mode of HCV p7 to that of influenza M2 shows two fundamentally different mechanisms of drug inhibition [Fig. 3(C)]. In the case of M2, one drug binds to one channel. Drug binding inhibits proton transport by directly blocking the channel passage and by preventing channel from opening. In the case of p7, rimantadine is clearly too small to block the channel. Instead, up to six drug molecules bind to the equivalent sites outside of the channel cavity. Drug binding to these sites may inhibit cation conduction by an allosteric mechanism, possibly by stabilizing the closed state of the channel.

Substrate interaction with transporters

When NOE measurements cannot be performed to characterize small molecule binding, a titration based approach using paramagnetic probes can reveal an approximate location of the binding site. We show below examples of substrate binding by *mitochondrial carriers*, which are a large family of MPs that catalyze the movement of metabolites, nucleotides, and inorganic phosphates across the mitochondrial inner membrane.[40,41] Mitochondrial carriers are relatively small compared to most transporters in the SoLute Carrier (SLC) group. The carriers generally have about 300 amino acids and can transport substrates as monomers.[42] Yet these relatively small scaffolds can afford selective transport of a large variety of substrates and can do so efficiently without disrupting the membrane potential.[43] Crystallography of mitochondrial carriers has been extremely slow, possibly due to the intrinsic conformational dynamics of these small transporters.

The uncoupling protein 2 (UCP2), which belongs to the UCP subfamily of mitochondrial carriers, was the first carrier protein for which a solution NMR sample was developed.[44] The UCPs are characterized by their ability to transport protons using fatty acids (FA).[45–47] In the case of UCP1, this activity causes proton leak across the inner membrane and is primarily responsible for heat generation in brown fat.[48–51] UCP-mediated proton transport can be blocked by purine nucleotides such as GDP.[52] UCP2 reconstituted in DPC/cardiolipin mixed micelles showed good NMR properties, for example, good resonance line-width, but spectral crowding due to threefold quasi symmetry precluded full-scale structure determination using NOEs. Instead, a low resolution backbone structure of UCP2 was derived using RDC-based molecular fragment searching and paramagnetic relaxation enhancement (PRE) restraints;[44] it showed a very similar fold to the AAC. In addition, the NMR system established for UCP2 provided a versatile platform for investigating the dynamic binding of free FA and GDP.

Berardi *et al*. used paramagnetic analogs of substrate or inhibitor to obtain PRE restraints to characterize substrate or ligand binding.[53] Although PREs are less precise, they can reveal proximal binding sites when NOEs cannot be obtained easily. For probing the FA (substrate) binding site in UCP2, the spin-labeled 5-doxyl-C18 FA (NO-FA) was used. Titration of NO-FA into UCP2 caused broadening of a small subset of backbone resonances, with the greatest PRE effects clustered around Gly281 on the lipid-facing side of the TM helix H6. In addition to the strongly broadened peaks, however, there were other regions that experienced weaker PRE due to partitioning of the long-chain FA in micelles, and it was not obvious which site was specific and functionally relevant. Interestingly, addition of GDP (inhibitor) to the sample containing UCP2 and NO-FA caused signal recovery of only certain residues while having little effect on the rest. Since GDP and FA had opposite effects on UCP2 activity, the region that showed peak recovery by GDP was proposed to be the functionally relevant FA binding site. Similarly, using nitroxide-labeled GDP (NO-GDP), it was shown by PRE measurements that GDP bound inside the polar cavity of UCP2. Together, the data showed that FA bound specifically to a peripheral site between TM helices H1 and H6 near the matrix side of UCP2 and that binding at this position was allosterically inhibited by the binding of GDP in the transporter central cavity. This rather qualitative structural information, obtained quickly by NMR, led to identification of critical mutations in UCP2 that abrogated FA or GDP binding. Testing these mutations in functional assays provided direct support for the previously proposed *protonaphoretic* mechanism:[54] UCPs catalyze the flipping of ionized FA partitioned in the membrane, which indirectly allows sustained shuttling of protons by FA across the membrane.[53]

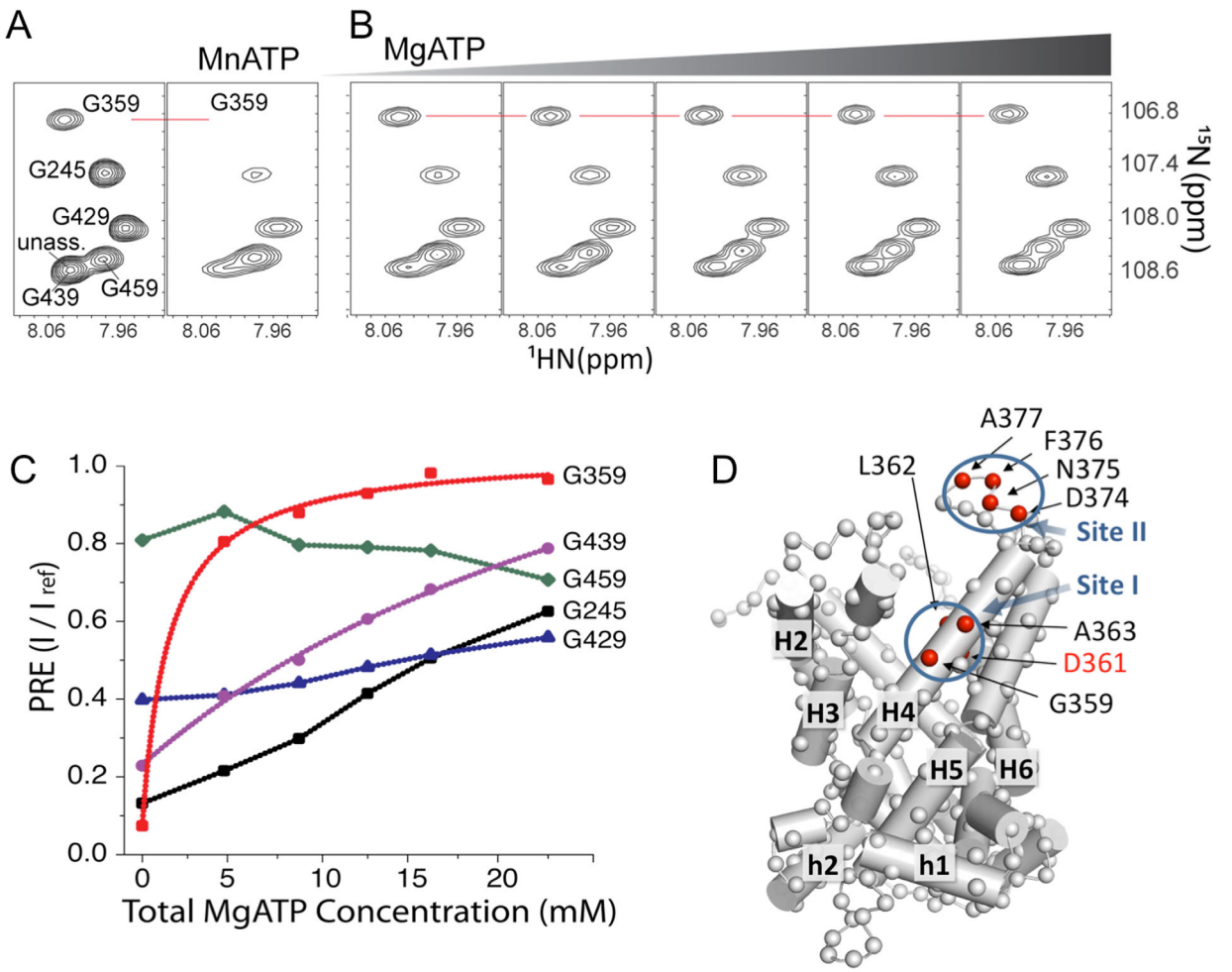

Figure 4. Investigating substrate binding to the SCaMC transporter domain by displacement titration. (A) A region of 2D ^{1}H–^{15}N TROSY–HSQC spectra of $SCaMC_{TMD}$ showing PRE effects of MnATP. Left and right panels correspond to spectra recorded with a 0.4 m*M* protein sample in the absence and presence of 1.25 m*M* MnATP, respectively. (B) The recovery of peaks broadened by MnATP after the addition of MgATP. The first panel shows the same spectral region as the right panel in (A). Panels 2–6 are spectra recorded at increasing concentrations of 4.5, 8.69, 12.5, 16.0, and 22.2 m*M* MgATP. (C) Plots of PRE (normalized peak intensity) versus MgATP concentration for the residues labeled as in (A). The peak intensity recovery data of only G359 and G439 could be fitted to the binding displacement equation (see text). (D) Mapping of significant PREs that could be specifically reduced by MgATP ($I_0 < 0.3$, $\Delta I_{max} > 0.3$ and $K_D < 2.5$ m*M*) (shown in red) on to the $SCaMC_{TMD}$ model.

In another study of substrate binding to carriers, Run *et al*. used paramagnetic ATP-Mn^{2+} to probe ATP-Mg^{2+} binding site in SCaMC, a calcium regulated carrier that selectively transports ATP-Mg^{2+}.[55] The SCaMC is one of the two carriers responsible for transporting ATP across the mitochondrial inner membrane. While the AAC accounts for the bulk ADP/ATP recycling in the matrix, the function of SCaMC is important for mitochondrial activities that depend on adenine nucleotides, such as gluconeogenesis and mitochondrial biogenesis.[56–60] Unlike AAC that selectively transports free ATP, SCaMC has strong selectivity for ATP-Mg^{2+} over free ATP, and the structural determinant of this selectivity remained elusive. Since the endogenous substrate of SCaMC is ATP-Mg^{2+}, it was convenient to substitute Mg^{2+} with paramagnetic Mn^{2+}.[55] Addition of ATP-Mn^{2+} to the carrier domain of SCaMC caused strong broadening of a subset of NMR peaks [Fig. 4(A)]. Manganese can bind nonspecifically to the phospholipids and acidic residues, causing nonspecific resonance broadening. Those ATP-Mn^{2+} molecules that bound specifically could, however, be specifically displaced by the nonparamagnetic ATP-Mg^{2+}, leading to the recovery of NMR resonances [Fig. 4(B,C)]. As a negative control, Mn^{2+} alone was added and also caused broadening of peaks, but none of these peaks were responsive to the addition of either Mg^{2+} or ATP-Mg^{2+}. The NMR signal recovery could be fitted to the $[P]_{tot}$[ATP-Mg]/([ATP-Mg] + K_D + [ATP-Mn]) curve, where K_D is the apparent dissociation constant and [ATP-Mg] and [ATP-Mn] are free substrate concentrations. The titration results revealed a binding site around Asp361 to which ATP-Mg^{2+} binds [Fig. 4(D)]. Functional mutagenesis showed that, indeed, mutating

Asp361 to tyrosine completely removed selectivity for ATP-Mg^{2+} over ATP in SCaMC.[55]

Allosteric Modulation of Membrane Protein Dynamics by Ligand

Modulation of protein energy landscape by specific ligands has been a recognized phenomenon in protein science for over five decades, and only since about 15 years ago has this problem been pursued in depth for a broad spectrum of proteins, most of them being water-soluble proteins.[61] These advances were attributed largely to the emergence of methods that can investigate higher energy states of proteins that are only transiently visited, for example, single molecule biophysics techniques and NMR relaxation dispersion measurements. Having evolved to transport materials or transmit signals across the membrane barrier, MP structures are expected to encode conformational dynamics that can be modulated by substrates or ligands. We describe below several examples in which NMR probes of different time scales are used to investigate how small molecule binding alters interstate transition for solute transporters, ion channel, and GPCRs.

Substrate facilitates interstate conversion of solute transporters

The NMR study of EmrE described above in "NMR Studies of Conformational Dynamics" demonstrated the elegant use of NMR ZZ-exchange spectroscopy to reveal the slow interconversion (5 s^{-1}) between the equally populated inward- and outward-facing states of the transporter when bound to the substrate TPP^+.[19] In a follow-up to this work, Morrison *et al*. used the same ZZ-exchange approach to investigate the influence of a variety of substrates (including those of the tetrahedral and planar scaffolds) on the exchange rate of EmrE.[62] They found that even within a limited set of seven substrates, the rate of interconversion between the inward- and outward-facing states of EmrE varies by three orders of magnitude.[62] The results indicate that substrate can strongly influence the energy landscape of EmrE, that is, changing the energy barrier between inward- and outward-facing states.

As mentioned earlier, EmrE has a pseudo-twofold symmetry, consistent with equal population of the inward- and outward-facing states of the asymmetric homodimer. The solute transporters belonging to the large family of mitochondrial carriers have a threefold longitudinal quasi-symmetry (symmetry axis perpendicular to the membrane) instead of the more common twofold symmetry.[63] Thus, the carriers might utilize a yet unknown mechanism that couples substrate binding and conformational exchange. The ADP/ATP carrier (AAC) has been the model system for structural and mechanistic studies of mitochondrial carriers because it remains, to date, the only carrier protein for which a high resolution crystal structure is available.[64,65] The crystal structure of AAC resembles an open-top barrel formed by three structurally similar domains in parallel orientation [Fig. 5(A)]. Each domain consists of two transmembrane helices separated by an amphipathic (AP) helix. The AAC crystal structure was obtained when the transporter was bound to the inhibitor CATR, and it represents the cytosol-facing open state (c-state) of the transporter as the cavity is only accessible from the intermembrane space. Other attempts to determine the structure of ligand-free AAC or the proposed matrix-facing open state (m-state) have not yet succeeded.

Brüschweiler and Yang *et al*. developed a sample of yeast AAC (yAAC3) reconstituted in DPC micelles which generated sufficiently high resolution spectrum when using deuterated protein and TROSY-based experiments [Fig. 5(B)]. The overall structural integrity of AAC in DPC micelles was demonstrated with NMR and isothermal titration calorimetry (ITC) of CATR binding. NMR titration of CATR showed a K_D of ~150 μM, and ITC experiment using an NMR sample with ~15 and ~40 times lower protein and detergent concentrations, respectively, yielded a K_D of ~20 μM. The larger K_D measured by NMR compared to ITC for CATR and ADP was due to the increased detergent concentration, as CATR is hydrophobic and partitions in empty detergent micelles. The authors conducted relaxation dispersion measurements at three different magnetic field strengths (600, 700, and 800 MHz) for the transporter in three different states: the free form, in the presence of the substrate ADP, and in the presence of the inhibitor CATR. The presence of a second, less populated state in equilibrium with the major state of a protein would lead to line broadening of the major state NMR peaks, and this effect can be modulated by applying a train of 180° radio-frequency (RF) pulses in the Carr–Purcell–Meiboom–Gill (CPMG) pulse sequence.[11,12] The shape of the resulting relaxation dispersion curve depends on the population of the two states (p_i), the chemical shift difference ($\Delta\omega$), and the rate of state interconversion (k_{ex}).[11,12]

For the free yAAC3, global CPMG fit yields K_{ex} ~870 ± 200 s^{-1} and relative populations of 98.0 ± 0.4% and 2.0 ± 0.4% for the two states at equilibrium. Since the NMR spectrum of the free yAAC3 is very similar to that of the CATR-bound yAAC3, the major population should be in the c-state (or the ground state). The c-state transiently converts to a lowly populated excited state. The first interesting observation was that despite the threefold quasi-symmetry of the AAC structure, the residues that show significant exchange are asymmetrically distributed [Fig. 5(C)]. The large exchanges are concentrated in domain I; the kink

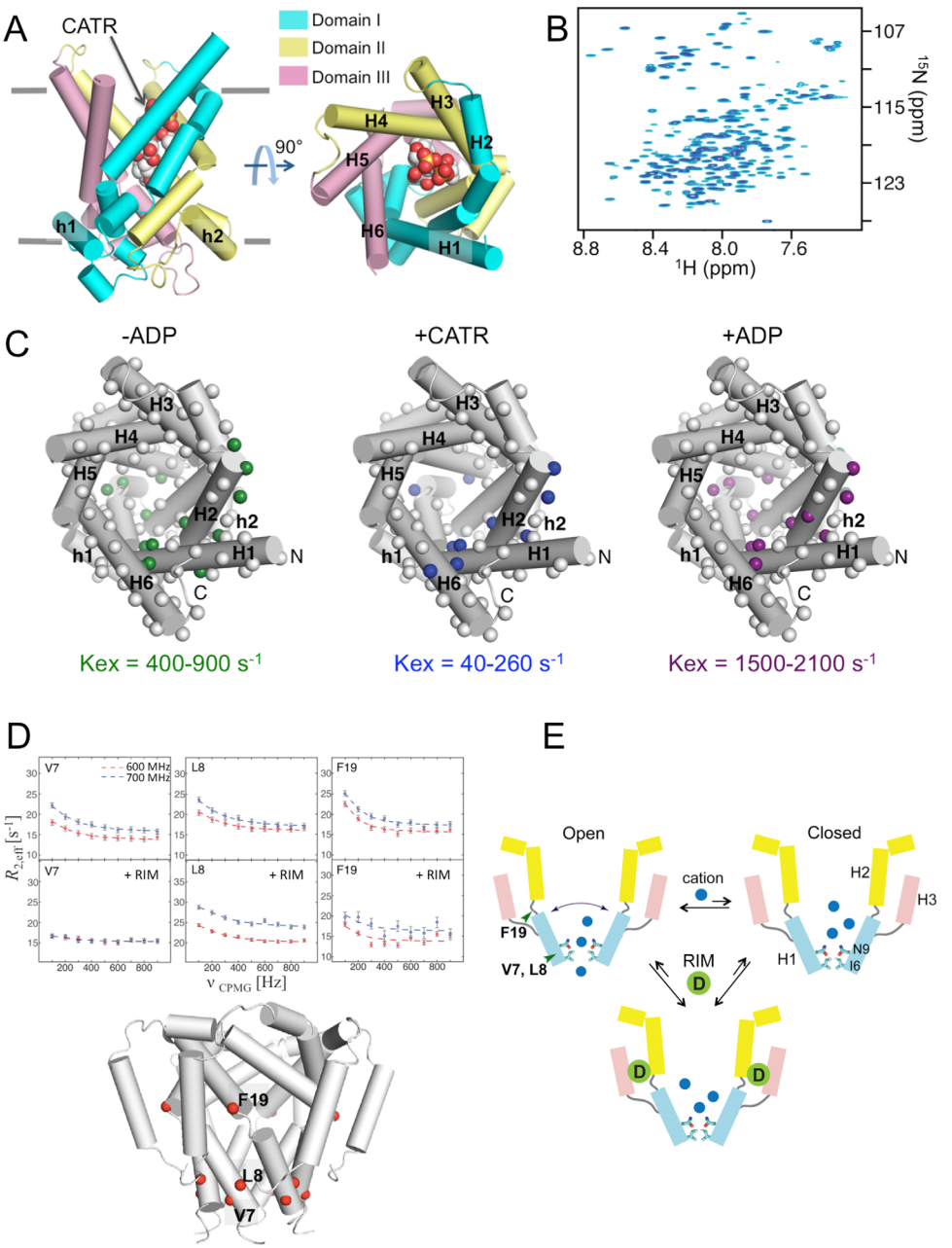

Figure 5. Allosteric modulation of membrane transport proteins by ligands. (A) The crystal structure of bovine AAC with bound CATR. The three pseudo symmetric domains are shown in cyan (Domain I), yellow (Domain II), and pink (Domain III). (B) The ^{1}H–^{15}N TROSY–HSQC spectrum of (^{15}N, ^{2}H)-labeled yeast AAC (yAAC3) reconstituted in DPC micelles. (C) The chemical-exchange maps of yAAC3 in the absence of ligands and in the presence of the inhibitor (CATR) or substrate (ADP). The colored spheres indicate significant chemical exchange with rates represented in different colors. Gray spheres represent residues with flat relaxation dispersion curves, or no chemical exchange. (D) CPMG relaxation dispersion curves for the p7 channel in the presence and absence of rimantadine (5 m*M*). Only three residues, V7, L8, and F19, showed significant chemical exchange in the absence of the drug, and these exchange rates were drastically suppressed by the binding of rimantadine. (E) Proposed "Molecular Wedge" model describing allosteric inhibition of the p7 channel by rimantadine.

region of H1 shows the strongest chemical exchange, for example, $\Delta\omega$ of Ala26 and Ser31 are 5.7 ± 0.9 and 5.5 ± 1.4 ppm in ^{15}N, respectively. Although there is no structural information on the excited state, the large chemical shift differences between the ground and excited states are indicative of a major conformational rearrangement in that region, suggesting that the excited state could be the elusive m-state. Another important observation was that addition of CATR or ADP did not alter $\Delta\omega$ distribution or relative state population of the transporter; it instead significantly changed the exchange rate. CATR binding slowed down conformational exchange by more than fivefold, consistent with the use of this

inhibitor to facilitate crystallization of AAC by making the protein less dynamic. In contrast to CATR, the substrate ADP increased the exchange rate from 870 ± 200 to 1800 ± 350 s^{-1}. The overall fast rate of exchange is compatible with AAC being a fast transporter (rate ~400 s^{-1} observed in liposome assays[66]). Although absolute exchange rates observed in detergent could have contained artifacts due to the transporter being in detergent micelles, the opposite modulation of the transporter rate by CATR and ADP should be qualitatively correct. This result suggests that the nucleotide substrate lowers the energy barrier between the c- and m-states probably by stabilizing the transition state between them.

Molecular wedge as viral ion channel blocker

As described in "Small Molecule Binding" above for the HCV p7 channel, the known inhibitor rimantadine binds to six equivalent peripheral pockets (due to the sixfold symmetry of the p7 hexamer) near the kink between the pore-forming helices H1 and H2, consisting of elements from different helical segments and from different subunits [Fig. 3(A)].[6] Since the drug binding site is away from the narrow constriction of the channel, it was not clear how drug binding inhibited cation conduction through the pore. Dev *et al*. performed relaxation dispersion measurement on p7 channel in DPC micelles using 2D CPMG TROSY–HSQC experiment at 600 and 700 MHz.[67] They found that while most of the channel did not show relaxation dispersion, residues at the H1–H2 hinge (Phe19) and the narrow end of the cavity (Val7, Leu8) experienced chemical exchanges (K_{ex} ~ 1000 ± 79 s^{-1} and ~10% excited state). This data is consistent with movements of the H1 helices that cause the tip of the funnel to open and close. According to the structure, such movements would induce large changes in the chemical environment of the hinge and the tip of the channel [Fig. 5(D)]. More importantly, addition of rimantadine slowed down motion at the tip of the channel, as relaxation dispersion curve for Val7, which has significant chemical exchange in the apo state, is completely flat in the drug-bound state. The dispersion curve of Phe19 is also significantly flatter, and individual curve fit yielded K_{ex} value of 67 ± 182 s^{-1}. Clearly, rimantadine binding makes the channel less dynamic. An important property of the drug binding site is that it consists of elements from different helical segments and from different subunits. The rimantadine may thus act as a "molecular wedge" that prevents the dynamic "breathing" of the channel required for ion conduction [Fig. 5(E)].

μ-opioid receptor: allosteric coupling between extracellular and intracellular domains

Allosteric modulation plays an important role in G-protein coupled receptor activation and signaling specificity.[68] In a recent work, Sounier *et al*. employed NMR to probe allosteric interactions between different domains of the μ-opioid receptor (μOR), a key player in pain management and drug addiction.[69] As many other GPCRs, μOR is activated by ligand binding in the extracellular pocket; the conformational change is then propagated to the cytoplasmic region where interaction with the heterotrimeric G-protein (in this case, an inhibitory G_i) initiates an intracellular signal transduction cascade. To analyze the activation signal propagation in μOR, the authors prepared a sample of lysine-dimethylated μOR in MNG detergent micelles. Lysine methylation has previously been shown to minimally perturb GPCR activity and to provide an excellent tool for the study of conformational change due to the favorable dynamic properties of fast rotating methyl groups.[70]

Methylated lysine ^{13}C HMQC of μOR was assigned by the analysis of the effect of single amino acid mutations and proteolysis on the spectra. Binding of a high-affinity agonist BU72 alone or both BU72 and a G-protein mimicking nanobody Nb33 to μOR did not significantly affect the NMR signal from the extracellular lysines (extracellular loop 2, ECL2), suggesting little conformational change in that region. However, the effect on the intracellular region was more significant. Peaks corresponding to lysines of the transmembrane helix 6 (TM6) in the apo-state disappeared, while new peaks corresponding to TM6 in the active conformation appeared upon addition of both BU72 and Nb33, but not of the agonist alone. The latter points to a relatively modest effect of ligand binding on conformational change of TM6, suggesting that G-protein binding (here mimicked by Nb33) plays an important role in the stabilization of the outward orientation of helix 6, a hallmark of GPCR activation.

Interestingly, lysine signals from two other cytoplasmic regions—intracellular loop 1 (ICL1) and the C-terminal amphipathic helix (H8)—were substantially broadened by BU72 alone and completely disappeared after the addition of both BU72 and Nb33. These results lend further support to the model of activation in which a G-protein is required to complete receptor transition to the active conformation initiated by ligand binding. Also, the stronger effect of BU72 on ICL1 and H8 compared to its effect on TM5 and TM6 suggests that the signal first propagates from the ligand binding pocket to ICL1 and H8 that may be involved in the initial complex formation with the G-protein. Complex formation then causes conformational changes in TM5 and TM6 observed in structures of activated GPCRs, an intriguing mechanistic hypothesis that still requires experimental verification.

Conclusions and Future Directions

Collectively, the examples discussed in this review demonstrate that the use of existing solution NMR

technologies can be quite effective in providing important insights into conformational dynamics and allostery of membrane channels, transporters, and receptors. The main challenge in these studies appeared to be the protein biochemistry needed to generate samples that are both active and amenable to multidimensional NMR experiments. One of the concerns surrounding solution NMR of membrane proteins has been the use of detergents with phosphocholine headgroups. The Foscholine detergents have been favored by NMR over detergents with sugar headgroups (widely used in crystallography) because they allow faster tumbling of the protein-micelle complexes in water, which, in turn, is due to weaker hydration of Foscholine compared to Maltoside and thus lower viscous drag in solution. But the Foscholine detergents typically have stronger denaturing potential due to the zwitterionic nature of phosphocholine headgroups. One approach here could therefore be to decrease the amount of detergent needed for protein solubilization by designing dimeric versions of Foscholines in analogy to neopentyl glycols, such as MNG, that proved to be extremely efficient in solubilizing GPCRs in functional form.[71] Same detergent-limiting strategy can be applied to bicelle formulations by using diheptanoyl phosphocholine with a tenfold lower CMC, as compared to the more conventional dihexanoyl.[72] As a completely detergent-free alternative, lipid nanodiscs have been developed as an attractive mimetic of native membranes[73] and small size nanodiscs have recently been developed to increase the molecular tumbling rate and improve the quality of the spectra.[74]

Another major technical challenge comes from the fact that many membrane channels, transporters and receptors show very inhomogeneous NMR resonance line-widths due to chemical exchange broadening, which is consistent with the dynamic nature of these membrane proteins. Therefore, spectroscopic approaches to minimize the adverse effect of chemical exchange on NMR spectra would significantly empower NMR applications to membrane protein. For example, the use of direct ^{15}N or ^{13}C detection[75,76] could potentially circumvent exchange broadening due to protons and complement conventional NMR by providing measurements for protein regions that have not been routinely analyzed by NMR. All these technological developments promise to greatly enhance solution NMR capability to provide a detailed view of functional dynamics of membrane embedded channels, transporters and receptors.

REFERENCES

1. Doyle DA, Morais Cabral J, Pfuetzner RA, Kuo A, Gulbis JM, Cohen SL, Chait BT, MacKinnon R (1998) The structure of the potassium channel: molecular basis of K+ conduction and selectivity. Science 280:69–77.
2. Van Horn WD, Kim HJ, Ellis CD, Hadziselimovic A, Sulistijo ES, Karra MD, Tian C, Sonnichsen FD, Sanders CR (2009) Solution nuclear magnetic resonance structure of membrane-integral diacylglycerol kinase. Science 324:1726–1729.
3. Zhou Y, Cierpicki T, Jimenez RH, Lukasik SM, Ellena JF, Cafiso DS, Kadokura H, Beckwith J, Bushweller JH (2008) NMR solution structure of the integral membrane enzyme DsbB: functional insights into DsbB-catalyzed disulfide bond formation. Mol Cell 31:896–908.
4. Gautier A, Mott HR, Bostock MJ, Kirkpatrick JP, Nietlispach D (2010) Structure determination of the seven-helix transmembrane receptor sensory rhodopsin II by solution NMR spectroscopy. Nat Struct Mol Biol 17:768–774.
5. Oxenoid K, Chou JJ (2005) The structure of phospholamban pentamer reveals a channel-like architecture in membranes. Proc Natl Acad Sci USA 102:10870–10875.
6. OuYang B, Xie S, Berardi MJ, Zhao X, Dev J, Yu W, Sun B, Chou JJ (2013) Unusual architecture of the p7 channel from hepatitis C virus. Nature 498:521–525.
7. Jaremko L, Jaremko M, Giller K, Becker S, Zweckstetter M (2014) Structure of the mitochondrial translocator protein in complex with a diagnostic ligand. Science 343:1363–1366.
8. Hiller S, Garces RG, Malia TJ, Orekhov VY, Colombini M, Wagner G (2008) Solution structure of the integral human membrane protein VDAC-1 in detergent micelles. Science 321:1206–1210.
9. Williamson JA, Cho SH, Ye J, Collet JF, Beckwith JR, Chou JJ (2015) Structure and multistate function of the transmembrane electron transporter CcdA. Nat Struct Mol Biol 22:809–814.
10. Schnell JR, Chou JJ (2008) Structure and mechanism of the M2 proton channel of influenza A virus. Nature 451:591–595.
11. Palmer AG, 3rd, Kroenke CD, Loria JP (2001) Nuclear magnetic resonance methods for quantifying microsecond-to-millisecond motions in biological macromolecules. Methods Enzymol 339:204–238.
12. Mittermaier A, Kay LE (2006) New tools provide new insights in NMR studies of protein dynamics. Science 312:224–228.
13. Chill JH, Louis JM, Baber JL, Bax A (2006) Measurement of 15N relaxation in the detergent-solubilized tetrameric KcsA potassium channel. J Biomol NMR 36: 123–136.
14. Chill JH, Louis JM, Miller C, Bax A (2006) NMR study of the tetrameric KcsA potassium channel in detergent micelles. Protein Sci 15:684–698.
15. Chill JH, Louis JM, Delaglio F, Bax A (2007) Local and global structure of the monomeric subunit of the potassium channel KcsA probed by NMR. Biochim Biophys Acta 1768:3260–3270.
16. Muth TR, Schuldiner S (2000) A membrane-embedded glutamate is required for ligand binding to the multidrug transporter EmrE. Embo J 19:234–240.
17. Ubarretxena-Belandia I, Baldwin JM, Schuldiner S, Tate CG (2003) Three-dimensional structure of the bacterial multidrug transporter EmrE shows it is an asymmetric Homodimer. Embo J 22:6175–6181.
18. Chen YJ, Pornillos O, Lieu S, Ma C, Chen AP, Chang G (2007) X-ray structure of EmrE supports dual topology model. Proc Natl Acad Sci USA 104:18999–19004.

19. Morrison EA, DeKoster GT, Dutta S, Vafabakhsh R, Clarkson MW, Bahl A, Kern D, Ha T, Henzler-Wildman KA (2012) Antiparallel EmrE exports drugs by exchanging between asymmetric structures. Nature 481:45–50.
20. Yildiz O, Vinothkumar KR, Goswami P, Kuhlbrandt W (2006) Structure of the monomeric outer-membrane porin OmpG in the open and closed conformation. Embo J 25:3702–3713.
21. Conlan S, Zhang Y, Cheley S, Bayley H (2000) Biochemical and biophysical characterization of OmpG: a monomeric porin. Biochemistry 39:11845–11854.
22. Zhuang T, Chisholm C, Chen M, Tamm LK (2013) NMR-based conformational ensembles explain pH-gated opening and closing of OmpG channel. J Am Chem Soc 135:15101–15113.
23. Iwahara J, Schwieters CD, Clore GM (2004) Ensemble approach for NMR structure refinement against (1)H paramagnetic relaxation enhancement data arising from a flexible paramagnetic group attached to a macromolecule. J Am Chem Soc 126:5879–5896.
24. Stewart EJ, Katzen F, Beckwith J (1999) Six conserved cysteines of the membrane protein DsbD are required for the transfer of electrons from the cytoplasm to the periplasm of *Escherichia coli*. Embo J 18:5963–5971.
25. Katzen F, Deshmukh M, Daldal F, Beckwith J (2002) Evolutionary domain fusion expanded the substrate specificity of the transmembrane electron transporter Dsbd. Embo J 21:3960–3969.
26. Deshmukh M, Brasseur G, Daldal F (2000) Novel Rhodobacter capsulatus genes required for the biogenesis of various c-type cytochromes. Mol Microbiol 35:123–138.
27. Yildirim MA, Goh KI, Cusick ME, Barabasi AL, Vidal M (2007) Drug–target network. Nat Biotechnol 25: 1119–1126.
28. Ishima R (2015) Protein-inhibitor interaction studies using NMR. Appl NMR Spectrosc 1:143–181.
29. O'Boyle NM, Banck M, James CA, Morley C, Vandermeersch T, Hutchison GR (2011) Open Babel: An open chemical toolbox. J Cheminformat 3:33.
30. Wang J, Schnell JR, Chou JJ (2004) Amantadine partition and localization in phospholipid membrane: a solution NMR study. Biochem Biophys Res Commun 324: 212–217.
31. Davies WL, Grunert RR, Haff RF, McGahen JW, Neumayer EM, Paulshock M, Watts JC, Wood TR, Hermann EC, Hoffmann CE (1964) Antiviral activity of 1-adamantanamine (amantadine). Science 144:862–863.
32. Griffin SD, Beales LP, Clarke DS, Worsfold O, Evans SD, Jaeger J, Harris MP, Rowlands DJ (2003) The p7 protein of hepatitis C virus forms an ion channel that is blocked by the antiviral drug, amantadine. FEBS Lett 535:34–38.
33. Griffin S, Stgelais C, Owsianka AM, Patel AH, Rowlands D, Harris M (2008) Genotype-dependent sensitivity of hepatitis C virus to inhibitors of the p7 ion channel. Hepatology 48:1779–1790.
34. Stouffer AL, Acharya R, Salom D, Levine AS, Di Costanzo L, Soto CS, Tereshko V, Nanda V, Stayrook S, DeGrado WF (2008) Structural basis for the function and inhibition of an influenza virus proton channel. Nature 451:596–599.
35. Cady SD, Schmidt-Rohr K, Wang J, Soto CS, Degrado WF, Hong M (2010) Structure of the amantadine binding site of influenza M2 proton channels in lipid bilayers. Nature 463:689–692.
36. Ohigashi Y, Ma C, Jing X, Balannick V, Pinto LH, Lamb RA (2009) An amantadine-sensitive chimeric BM2 ion channel of influenza B virus has implications for the mechanism of drug inhibition. Proc Natl Acad Sci USA 106:18775–18779.
37. Pielak RM, Oxenoid K, Chou JJ (2011) Structural investigation of rimantadine inhibition of the AM2–BM2 chimera channel of influenza viruses. Structure 19:1655–1663.
38. Steinmann E, Whitfield T, Kallis S, Dwek RA, Zitzmann N, Pietschmann T, Bartenschlager R (2007) Antiviral effects of amantadine and iminosugar derivatives against hepatitis C virus. Hepatology 46:330–338.
39. Pavlovic D, Neville DC, Argaud O, Blumberg B, Dwek RA, Fischer WB, Zitzmann N (2003) The hepatitis C virus p7 protein forms an ion channel that is inhibited by long-alkyl-chain iminosugar derivatives. Proc Natl Acad Sci USA 100:6104–6108.
40. Palmieri F, Agrimi G, Blanco E, Castegna A, Di Noia MA, Iacobazzi V, Lasorsa FM, Marobbio CM, Palmieri L, Scarcia P, Todisco S, Vozza A, Walker J (2006) Identification of mitochondrial carriers in *Saccharomyces cerevisiae* by transport assay of reconstituted recombinant proteins. Biochim Biophys Acta 1757:1249–1262.
41. Klingenberg M (2009) Cardiolipin and mitochondrial carriers. Biochim Biophys Acta 1788:2048–2058.
42. Bamber L, Harding M, Monne M, Slotboom DJ, Kunji ER (2007) The yeast mitochondrial ADP/ATP carrier functions as a monomer in mitochondrial membranes. Proc Natl Acad Sci USA 104:10830–10834.
43. Kunji ER, Robinson AJ (2010) Coupling of proton and substrate translocation in the transport cycle of mitochondrial carriers. Curr Opin Stuct Biol 20:440–447.
44. Berardi MJ, Shih WM, Harrison SC, Chou JJ (2011) Mitochondrial uncoupling protein 2 structure determined by NMR molecular fragment searching. Nature 476:109–113.
45. Cannon B, Hedin A, Nedergaard J (1982) Exclusive occurrence of thermogenin antigen in brown adipose tissue. FEBS Lett 150:129–132.
46. Lin CS, Klingenberg M (1980) Isolation of the uncoupling protein from brown adipose tissue mitochondria. FEBS Lett 113:299–303.
47. Lin CS, Klingenberg M (1982) Characteristics of the isolated purine nucleotide binding protein from brown fat mitochondria. Biochemistry 21:2950–2956.
48. Rafael J, Ludolph HJ, Hohorst HJ (1969) [Mitochondria from brown adipose tissue: uncoupling of respiratory chain phosphorylation by long fatty acids and recoupling by guanosine triphosphate]. Hoppe-Seyler's Zeitschrift Physiol Chem 350:1121–1131.
49. Nicholls DG (1979) Brown adipose tissue mitochondria. Biochim Biophys Acta 549:1–29.
50. Klingenberg M (2010) Wanderings in bioenergetics and biomembranes. Biochim Biophys Acta 1797:579–594.
51. Krauss S, Zhang CY, Lowell BB (2005) The mitochondrial uncoupling–protein homologues. Nat Rev Mol Cell Biol 6:248–261.
52. Jaburek M, Varecha M, Gimeno RE, Dembski M, Jezek P, Zhang M, Burn P, Tartaglia LA, Garlid KD (1999) Transport function and regulation of mitochondrial uncoupling proteins 2 and 3. J Biol Chem 274:26003–26007.
53. Berardi MJ, Chou JJ (2014) Fatty acid flippase activity of UCP2 is essential for its proton transport in mitochondria. Cell Metab 20:541–552.
54. Garlid KD, Orosz DE, Modriansky M, Vassanelli S, Jezek P (1996) On the mechanism of fatty acid-induced

proton transport by mitochondrial uncoupling protein. J Biol Chem 271:2615–2620.
55. Run C, Yang Q, Liu Z, OuYang B, Chou JJ (2015) Molecular basis of MgATP selectivity of the mitochondrial SCaMC carrier. Structure 23:1394–1403.
56. Pollak JK, Sutton R (1980) The transport and accumulation of adenine nucleotides during mitochondrial biogenesis. Biochem J.
57. Aprille JR (1988) Regulation of the mitochondrial adenine nucleotide pool size in liver: mechanism and metabolic role. Faseb J 2:2547–2556.
58. Schild L, Blair PV, Davis WI, Baugh S (1999) Effect of adenine nucleotide pool size in mitochondria on intramitochondrial ATP levels. Biochim Biophys Acta.
59. Traba J, Del Arco A, Duchen MR, Szabadkai G, Satrustegui J (2012) SCaMC-1 promotes cancer cell survival by desensitizing mitochondrial permeability transition via ATP/ADP-mediated matrix Ca(2+) buffering. Cell Death Differ 19:650–660.
60. Satrú Stegui J, Pardo B, del Arco A (2007) Mitochondrial transporters as novel targets for intracellular calcium signaling. Physiol Rev 87:29–67.
61. Swain JF, Gierasch LM (2006) The changing landscape of protein allostery. Curr Opin Struct Biol 16:102–108.
62. Morrison EA, Henzler-Wildman KA (2014) Transported substrate determines exchange rate in the multidrug resistance transporter EmrE. J Biol Chem 289:6825–6836.
63. Shi Y (YEAR) Common folds and transport mechanisms of secondary active transporters. Ann Rev Biophys 42:51–72.
64. Pebay-Peyroula E, Dahout-Gonzalez C, Kahn R, Trezeguet V, Lauquin GJ, Brandolin G (2003) Structure of mitochondrial ADP/ATP carrier in complex with carboxyatractyloside. Nature 426:39–44.
65. Ruprecht JJ, Hellawell AM, Harding M, Crichton PG, McCoy AJ, Kunji ER (YEAR) Structures of yeast mitochondrial ADP/ATP carriers support a domain-based alternating-access transport mechanism. Proc Natl Acad Sci USA 111:E426–E434.
66. Gropp T, Brustovetsky N, Klingenberg M, Muller V, Fendler K, Bamberg E (1999) Kinetics of electrogenic transport by the ADP/ATP carrier. Biophys J 77:714–726.
67. Dev J, Bruschweiler S, Ouyang B, Chou JJ (2015) Transverse relaxation dispersion of the p7 membrane channel from hepatitis C virus reveals conformational breathing. J Biomol NMR 61:369–378.
68. Christopoulos A (2014) Advances in G protein-coupled receptor allostery: from function to structure. Mol Pharmacol 86:463–478.
69. Sounier R, Mas C, Steyaert J, Laeremans T, Manglik A, Huang W, Kobilka BK, Demene H, Granier S (2015) Propagation of conformational changes during mu-opioid receptor activation. Nature 524:375–378.
70. Bokoch MP, Zou Y, Rasmussen SG, Liu CW, Nygaard R, Rosenbaum DM, Fung JJ, Choi HJ, Thian FS, Kobilka TS, Puglisi JD, Weis WI, Pardo L, Prosser RS, Mueller L, Kobilka BK (2010) Ligand-specific regulation of the extracellular surface of a G-protein-coupled receptor. Nature 463:108–112.
71. Chae PS, Rasmussen SG, Rana RR, Gotfryd K, Kruse AC, Manglik A, Cho KH, Nurva S, Gether U, Guan L, Loland CJ, Byrne B, Kobilka BK, Gellman SH (2012) A new class of amphiphiles bearing rigid hydrophobic groups for solubilization and stabilization of membrane proteins. Chemistry 18:9485–9490.
72. Lu Z, Van Horn WD, Chen J, Mathew S, Zent R, Sanders CR (2012) Bicelles at low concentrations. Mol Pharmaceut 9:752–761.
73. Denisov IG, Grinkova YV, Lazarides AA, Sligar SG (2004) Directed self-assembly of monodisperse phospholipid bilayer nanodiscs with controlled size. J Am Chem Soc 126:3477–3487.
74. Hagn F, Etzkorn M, Raschle T, Wagner G (2013) Optimized phospholipid bilayer nanodiscs facilitate high-resolution structure determination of membrane proteins. J Am Chem Soc 135:1919–1925.
75. Takeuchi K, Arthanari H, Imai M, Wagner G, Shimada I (2016) Nitrogen-detected TROSY yields comparable sensitivity to proton-detected TROSY for nondeuterated, large proteins under physiological salt conditions. J Biomol NMR.
76. Takeuchi K, Sun ZY, Wagner G (2008) Alternate 13C–12C labeling for complete mainchain resonance assignments using C alpha direct-detection with applicability toward fast relaxing protein systems. J Am Chem Soc 130:17210–17211.